analytical chemistry

Article

pubs.acs.org/ac

Virus-Enabled Biosensor for Human Serum Albumin

Alana F. Ogata,[†] Joshua M. Edgar,[†] Sudipta Majumdar,[†] Jeffrey S. Briggs,[‡] Shae V. Patterson,[‡] Ming X. Tan,[§] Stephan T. Kudlacek,[†] Christine A. Schneider,[†] Gregory A. Weiss,*[,†,‡] and Reginald M. Penner*[,†,‡]

[†]Department of Chemistry, University of California, Irvine, Irvine, California 92697-2025, United States

[‡]PhageTech Inc., 5151 California Avenue, Suite 150, Irvine, California 92617, United States

[§]Wainamics Inc., 3135 Osgood Court, Fremont, California 94539, United States

Supporting Information

ABSTRACT: The label-free detection of human serum albumin (HSA) in aqueous buffer is demonstrated using a simple, monolithic, two-electrode electrochemical biosensor. In this device, both millimeter-scale electrodes are coated with a thin layer of a composite containing M13 virus particles and the electronically conductive polymer poly(3,4-ethylenedioxy thiophene) or PEDOT. These virus particles, engineered to selectively bind HSA, serve as receptors in this biosensor. The resistance component of the electrical impedance, Z_{re}, measured between these two electrodes provides electrical transduction of HSA binding to the virus-PEDOT film. The analysis of sample volumes as small as 50 μL is made possible using a microfluidic cell. Upon exposure to HSA, virus-PEDOT films show a prompt increase in Z_{re} within 5 s and a stable Z_{re} signal within 15 min. HSA concentrations in the range from 100 nM to 5 μM are detectable. Sensor-to-sensor reproducibility of the HSA measurement is characterized by a coefficient-of-variance (COV) ranging from 2% to 8% across this entire concentration range. In addition, virus-PEDOT sensors successfully detected HSA in synthetic urine solutions.

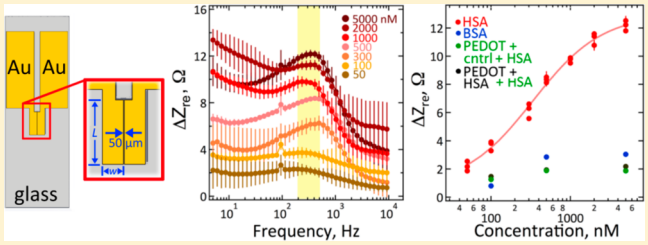

A new approach to the point-of-care (PoC) detection of protein disease markers involves the use of virus particles, rather than antibodies, within a bioaffinity capture layer. Relative to antibodies, virus particles have several advantages that make them attractive for emerging PoC sensor technologies: First, virus particles can be engineered to bind virtually any protein, even toxic proteins for which antibody development is difficult.[1,2] Second, virus particles are less thermally and chemically labile than antibodies, dramatically simplifying the large-scale production, storage, and transport of biosensors that rely on virus-based bioaffinity layers.[3] Finally, virus particles that are capable of antibody-like affinities can be produced in quantity at lower costs.[4]

Here we describe a PoC biosensor that exploits electrodeposited bioaffinity layers that consist of a composite of virus particles with an electrically conductive polymer, poly(3,4-ethylenedioxythiophene) or PEDOT. The receptors in these biosensors are M13 virus particles. On the surface of these M13 virus particles, peptides are "displayed" as fusions to the N-terminus of a subset of this virus' major P8 coat proteins that compose the virus capsid. From libraries of $>10^{11}$ unique sequences, the displayed peptide on the virus surface is selected on the basis of its target binding affinity and specificity. The use of whole virus particles as a bioaffinity matrix for biosensors dates to 2003, when it was demonstrated that an engineered M13 virus could be immobilized by physisorption onto the gold transducer of an acoustic wave sensor[5] and, somewhat later,[6] to a gold quartz crystal microbalance electrode, enabling the detection in both cases of β-galactosidase.[5,6] Subsequently, in 2007 Cosnier et al.[7] demonstrated biosensors based on the virus T7 capable of detecting human antibodies to the West Nile virus.

Virus-PEDOT films provide a simple and reproducible method for immobilizing virus on an electrode that involves entraining it in a film of the conductive polymer PEDOT. We have demonstrated two types of biosensors based upon this bioaffinity matrix: virus-PEDOT nanowires prepared using the lithographically patterned nanowire electrodeposition (LPNE) process,[8,9] and virus-PEDOT films on planar gold electrodes.[10,11] Biosensors based upon virus-PEDOT nanowires transduce target binding using the through-nanowire resistance[8,9] whereas films of virus-PEDOT use electrical impedance spectroscopy (EIS) without added redox species to transduce the binding of a target molecule to the virus-PEDOT composite.[10,11] We have demonstrated that virus-PEDOT biosensors can detect prostate specific membrane antigen (PSMA), a 90 kDa glycoprotein that is a promising prostate cancer marker, with a limit-of-detection in synthetic urine of 0.50 nM.[11] These experiments establish the current baseline capabilities for this technology in terms of its sensitivity and

Received: December 6, 2016
Accepted: December 19, 2016
Published: December 19, 2016

DOI: 10.1021/acs.analchem.6b04840
Anal. Chem. 2017, 89, 1373−1381

Table 1. Summary of Related Biosensing Literature Involving Virus Biosensors and/or HSA

detection method[a]	analyte	bioaffinity surface	range	LOD_{exptl}	inter/intraassay	total analysis time	ref
immuno-inhibition assay	HSA	PCS modified latex particles incorporating HSA antibody	75.19 nM−3.76 μM	6.02 nM (calcd)	inter <10% N = 20	N/A	23
QCM	HSA	quartz crystal coated with polystyrene solution for direct HSA antibody adsorption	15.04 nM−3.76 μM	15.04 nM (meas)	N/A	2 h	24
EIS	HSA	HSA antibody immobilized on functionalized Si_3N_4 substrate	10 pM−10 μM	0.1 fM (calcd)	inter 7.6% N = 3	1 h	25
DPV and EIS ($Fe(CN)_6$)	HSA (blood sample)	HSA molecularly imprinted polymer	DPV, 12 nM−300 nM; EIS, 60 nM−1200 nM	DPV, 249 pM (calcd); EIS, 12 nM (calcd)	N/A	1 h	26
DPV	HSA	HSA antibody modified gold nanoparticles immobilized on screen printed carbon electrode surfaces	37 nM−3 μM	376 pM (calcd)	intra 3.5% N = 8; inter 5% N = 3	N/A	27
EIS	HSA	modified glass surface with 3-aminopropyltriethoxysilane and HSA antibody in between two gold electrodes	3.01 nM−90 μM	3 nM (meas)	N/A	1 h	28
EIS ($Fe(CN)_6$)	cancer cells	octapeptide fused phage immobilized by layer-by-layer assembly onto gold electrodes	200−2.0E8 cells/mL	79 cells/mL (calcd)	inter 4.9% N = 5	1 h	29
EIS ($Fe(CN)_6$)	HSA	HSA antibodies immobilized onto electropolymerized polytyramine films using a glutaraldehyde cross-linker	27.6 pM−5.54 nM	24 pM (calcd)	inter 9.2% N = 4; intra 11.4% N = 5	50 min	30
EIS	HSA	virus-PEDOT composite film	100 nM−5 μM	100 nM (meas)	intra 1.71−3.9% N = 5; inter 2%-8% N = 3	<10 min	this work

[a]Abbreviations: HSA, human serum albumin; BSA, bovine serum albumin; QSM, quartz crystal microbalance; EIS, electrochemical impedance spectroscopy; DPV, differential pulse voltammetry; PCS, poly(chloromethyl)styrene; PEDOT, poly(3,4-thiophene).

DOI: 10.1021/acs.analchem.6b04840
Anal. Chem. 2017, 89, 1373−1381

limit-of-detection. However, research grade gold electrodes, three-electrode potentiostats, and stand-alone reference and counter electrodes were employed in this prior work. How can this sensing modality be translated into manufacturable and miniaturizable biosensor architectures and how well do these work in terms of sensitivity, signal-to-noise, and sensor-to-sensor reproducibility? We address these issues here for a problem of broad importance.

The analyte of interest in this study is human serum albumin (HSA, MW = 66.5 kDa) in urine. HSA is a well-established urinary biomarker that can indicate a wide range of adverse health conditions such as stroke, coronary artery disease, heart disease, renal disease, and liver or kidney failure, especially for those with diabetes.[12] In healthy adults, HSA is excreted in urine at a concentration below 20 mg/mL (or 300 nM).[13−15] HSA levels of 20−200 mg/L (300 nM to 3 μM) indicate microalbuminuria, a moderate increase in albumin related to a risk of kidney disease,[16,17] and patients with HSA concentrations above 200 mg/L are diagnosed with macroalbuminuria.[13,18] Current dipstick tests are only sensitive to macroalbuminuria, a diagnosis that usually occurs when kidney disease has irreversibly progressed to kidney failure.[16] Specifically, there is a need for a urinalysis test for HSA that is able to detect the protein from <20 mg/L to >200 mg/L corresponding to <300 nM to >3 μM. In this study, we describe the label-free detection of HSA in aqueous buffer and synthetic urine using a simple, monolithic, two-electrode electrochemical biosensor. A comparison of the current work compared to relevant prior biosensor studies is summarized in Table 1.

EXPERIMENTAL SECTION

Materials and Methods. Procedures associated with materials, phage library design and selection of HSA binders, device fabrication, and AFM and SEM analysis are described in the Supporting Information.

Synthesis of Virus-PEDOT Films. Gold-film electrodes and flow cells were cleaned by O_2 plasma for 10 min prior to electroplating. The flow cell was then mounted on the gold-film electrodes. A flame-cleaned platinum foil counter electrode, wrapped around a mercurous sulfate electrode (MSE), was used during electropolymerization. Film growth occurred by cycling between +0.20 V and +0.80 V using a PalmSens3 controlled by PS-Trace software (PalmSens BV, Houten, Netherlands) at a scan rate of 20 mV/s in plating solution. Gold-film electrodes were first exposed to EDOT plating solution (12.5 mM $LiClO_4$, 2.5 mM EDOT) for 2 cycles of electropolymerization. Electrodes were then exposed to virus-EDOT plating solution (8 nM M13 virus, 12.5 mM $LiClO_4$, 2.5 mM EDOT) and electropolymerized for 2 cycles. Electropolymerization of virus-EDOT was repeated with new virus-EDOT plating solution three times for a total of 8 cycles.

Electrochemical Impedance Spectroscopy. Various concentrations of HSA in run buffer (casein, Tween, PBS) were prepared immediately prior to exposure of virus electrodes. Newly plated virus-PEDOT films were exposed to blocking solution (casein, PBS) for 15 min followed by rinsing with wash buffer (PBS, Tween). The electrode was then rinsed three times with run buffer and allowed to equilibrate while monitoring the impedance signal over time. Equilibrium was defined as an impedance drift of <0.5 Ω/min over a two minute period. After equilibrium was attained, five consecutive EIS measurements were taken using a PalmSens3 controlled by PS-Trace software (PalmSens BV, Houten, Netherlands). The amplitude of the applied voltage was 10 mV, and 50 data points were acquired spanning a frequency range of 5 Hz to 40 kHz. Virus electrodes were then exposed to HSA solutions in run buffer, monitored for equilibration, and five consecutive EIS measurements were collected. Independent electrodes were used for EIS measurements of HSA solutions and BSA solutions for a positive and negative response, respectively.

RESULTS AND DISCUSSION

Electrodeposition and Characterization of Virus-PEDOT Films. We describe a biosensor that consists of a pair of gold electrodes lithographically patterned onto a microscope slide, mated to a flow cell (Figure 1a). The flow

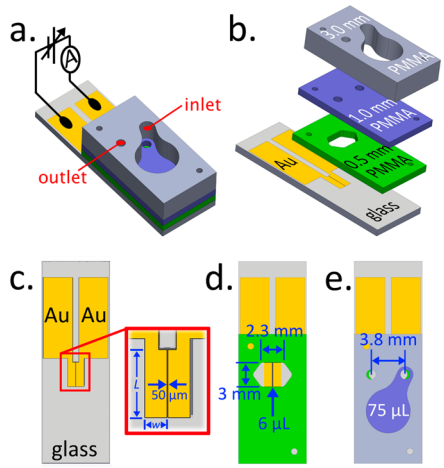

Figure 1. Schematic diagrams of the biosensor and the flow cell described in this study. (a) An assembled flow cell attached to a gold-electrode device consists of two gold contacts connected to a potentiostat for EIS measurements. (b) A gold-electrode device and detailed structure of a single PMMA flow cell. (c) A single device with a red box showing the two planar gold electrodes used for sensing. The two gold electrodes have a length (L) of 2 mm and width (w) of 0.85 mm, and are separated by a 50 μm gap. (d) Dimensions of the first PMMA flow cell layer which creates a cell holding 6 μL of solution over the gold electrodes. (e) Top view representation of assembled flow cell. Solution flows from the inlet port (right), through the cell, and exits through the outlet port (left) into a reservoir with a 75 μL capacity.

cell, in three parts, is assembled on the sensor electrode before electrodeposition of the virus-PEDOT bioaffinity layer (Figure 1b). Each of the two gold electrodes is 1 mm × 3 mm, and the two electrodes are separated by 50 μm (Figure 1c). These electrodes span the 3 mm width of the flow channel from edge to edge, and are centered along its 2.3 mm length (Figure 1d). Plating and sample solutions are introduced into the 75 μL reservoir at top (Figure 1e), and the 6 μL volume of the flow channel quickly fills by capillary action. Both gold electrodes are modified with identical virus-PEDOT films that serve as bioaffinity layers. The virus incorporated into the PEDOT film is engineered[19] to selectively bind HSA with an apparent K_D in the 10−100 nM range, as estimated using enzyme-linked immunosorbent assay (ELISA, Figure S2).

The sensor operates without counter and reference electrodes, but these additional electrodes were used for the electrodeposition of virus-PEDOT films. Both virus-PEDOT films were electrodeposited simultaneously using an aqueous plating solution containing 8 nM virus, 2.5 mM EDOT, and

DOI: 10.1021/acs.analchem.6b04840
Anal. Chem. 2017, 89, 1373−1381

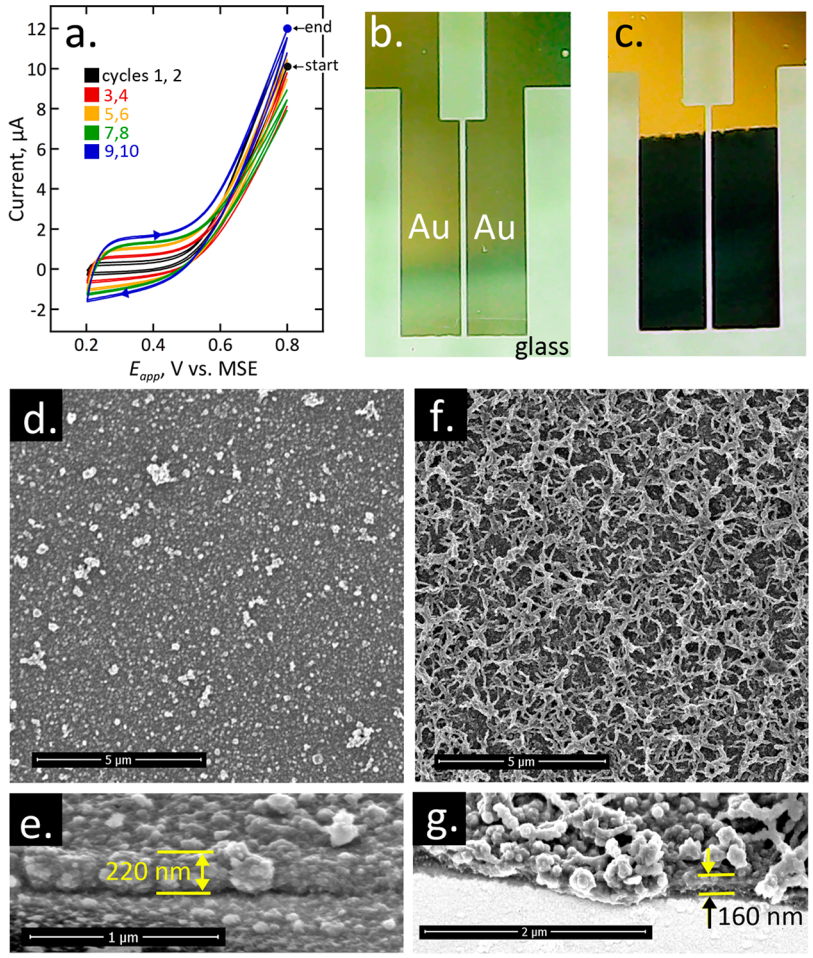

Figure 2. Electrodeposition and SEM characterization of virus-PEDOT bioaffinity coatings. (a) Electrodeposition of a virus-PEDOT film by cyclic voltammetry. Film prepared by two cycles in aqueous EDOT solution (2.5 mM EDOT, 12.5 mM $LiClO_4$) followed by eight cycles in a virus-EDOT solution (2.5 mM EDOT, 12.5 mM $LiClO_4$, 8 nM HSA virus). Virus-EDOT solution was replenished every two cycles. All scan rates were 20 mV/s. Optical image of (b) bare gold electrodes and (c) gold electrodes after electrodeposition of virus-PEDOT film. (d–g) Scanning electron microscopy images of uncoated films. (d) PEDOT film prepared by 10 consecutive cycles of deposition in aqueous EDOT solution (2.5 mM EDOT, 12.5 mM $LiClO_4$). (e) PEDOT edge showing film height of approximately 220 nm. (f) Virus-PEDOT film prepared as described in part a showing dense incorporation of phage bundles on the surface. (g) Virus-PEDOT edge showing primer layer of PEDOT with thickness of approximately 160 nm and PEDOT-coated phage on top.

12.5 mM $NaClO_4$. Ten voltammetric scans from +0.80 V to +0.20 V versus MSE (Figure 2a) used were for the preparation of each pair of films, and the plating solution within the flow cell, which was quiescent during the deposition process, was replaced every two cycles. Electrodeposited virus-PEDOT films were a uniform dark blue in color (Figure 2b,c).

Scanning electron micrographs of pure PEDOT films prepared from the same plating solution without the addition of virus (Figure 2d) show a textured surface, dotted with 50–500 nm diameter protrusions. The apparent film thickness measured in the SEM is in the 200–300 nm range (Figure 2e). Virus-PEDOT films prepared from plating solution containing added 8 nM virus showed a surface with much greater roughness; the filamentous texture observed is characteristic of the virus-PEDOT composite (Figure 2f). At the film edge, SEM images acquired at high angular incidence of the electron beam show that a thin PEDOT layer of ≈150–180 nm is present on the gold surface, and virus particles protrude from this PEDOT base layer like a shag carpet (Figure 2g). Several SEM images were obtained at random spots on the PEDOT-phage films and were visually identical, showing complete and uniform coverage over the gold electrodes.

In comparison to previous reports,[10] refreshing the plating solution every two scans dramatically increased the amount of virus present in the resulting virus-PEDOT films, as qualitatively assessed from these SEM images (Figure 2d,f). The observed depression in phage loading after just two plating cycles suggests that virus particles diffuse slowly to the surface of the electrode and are depleted within two cycles of deposition. An increase in virus loading enables high density of receptors on the virus-PEDOT sensors.

Atomic force microscopy (AFM) images of PEDOT-only films prepared using this procedure (Figure 3a) allow for determination of the RMS surface roughness which is 15 nm. At the edges of the gold electrode (Figure 3a, right), the film thickness could be determined, and was in the range 350–450 nm, significantly thicker than that measured in the high vacuum environment of the SEM. We attribute the difference to the removal of water associated with film swelling in the SEM whereas films imaged by AFM were not subjected to high vacuum and likely retain a greater water content as a result.

DOI: 10.1021/acs.analchem.6b04840
Anal. Chem. 2017, 89, 1373–1381

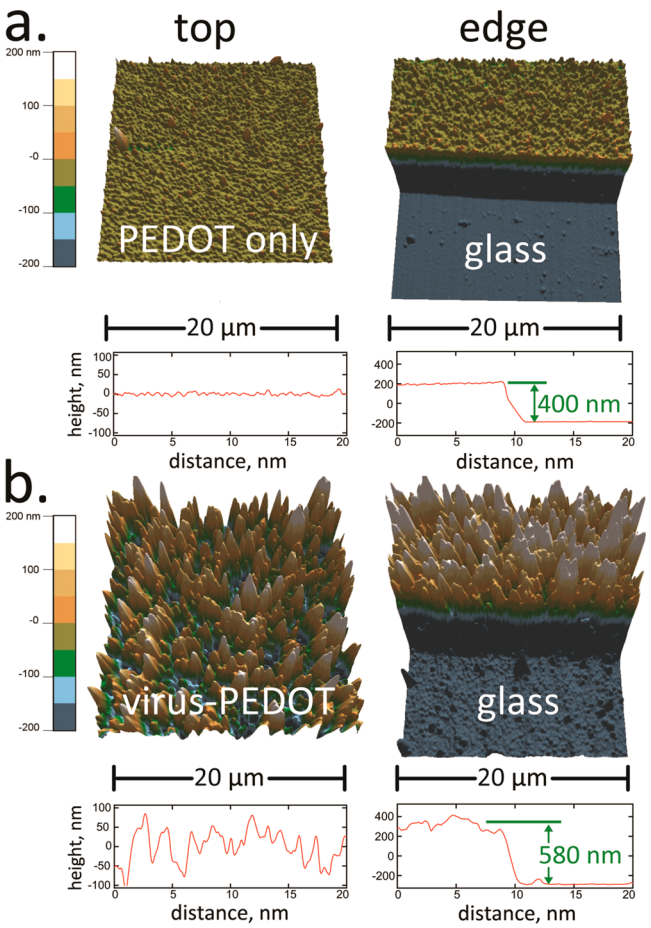

Figure 3. Atomic force microscopy of virus-PEDOT bioaffinity films and AFM line scans shown at the bottom. (a) PEDOT-only film prepared by 10 cycles of deposition in EDOT solution (2.5 mM EDOT, 12.5 mM $LiClO_4$). Topography of the middle (left) and the edge (right) of films imaged by atomic force microscopy. The film-edge height shown in line scans includes the gold electrode layer (60 nm). (b) Virus-PEDOT film prepared by two cycles of deposition in EDOT solution followed by eight cycles in virus-EDOT solution (2.5 mM EDOT, 12.5 mM $LiClO_4$, 8 nM HSA virus), with virus-EDOT solution replenished every two cycles. The rms roughness for PEDOT and virus-PEDOT films is ≈10 and ≈150 nm, respectively.

AFM images of virus-PEDOT films (Figure 3b) show a much more pronounced topography and a greater RMS roughness of 101 nm. The apparent film thickness for these films (Figure 3b, right) is in the range 550−650 nm, but this value includes the PEDOT film and the protruding virus layer, that cannot be distinguished in these images.

Detection of HSA in Buffer. We begin by comparing the impedance response of virus-PEDOT biosensors in BSA and HSA in order to ascertain the degree to which HSA can be selectively detected. BSA and HSA are identical in size (66.5 kDa) and have 76% sequence homology, so this comparison provides a challenging test for HSA selectivity.[20] Nyquist plots (Z_{im} vs Z_{re}) for virus-PEDOT films immersed in run buffer (Figure 4a) show behavior characteristic of a series RC circuit, as expected. An equivalent circuit for the virus-PEDOT film quantitatively accounting for these observations is presented in the Supporting Information. The addition of 500 nM BSA to the buffer causes a slight, 1−4 Ω, shift in this curve to higher Z_{re}, but almost no change in Z_{im}. For a different virus-PEDOT film (Figure 4b), a larger shift in Z_{re} of 8−10 Ω is observed upon exposure to 500 nM HSA in buffer, and a much smaller shift is seen in Z_{im}. In the subsequent discussion, we refer to the shifts in Z_{re} and Z_{im} relative to buffer as ΔZ_{re} and ΔZ_{im}. Plots of ΔZ_{re} and ΔZ_{im} versus frequency (Figure 4c,d) show that ΔZ_{re} is superior to ΔZ_{im} for detecting HSA at 500 nM across the entire frequency spectrum from 5 Hz to 10 kHz. The error bars shown in these two plots represent the standard deviation of the mean for multiple impedance measurements (n = 5) on a single biosensor. The measurement-to-measurement dispersion in impedance seen both for ΔZ_{re} and ΔZ_{im} is simply noise, and a signal-to-noise ratio (S/N) can therefore be calculated at each frequency point as $\Delta Z_{re}/\sigma_{re}$ and $\Delta Z_{im}/\sigma_{im}$ (Figure 4e,f) where σ_{re} is the standard deviation of ΔZ_{re} across these five EIS measurements at each frequency. These plots show that for ΔZ_{re} (Figure 4e) a S/N of 50 is obtained at 500−600 Hz for HSA whereas BSA at the same 500 nM concentration and frequency is detected with a S/N of 1−3. For ΔZ_{im}, on the other hand (Figure 4f), both HSA and BSA produce a comparable S/N ranging from 10 to 50 across the frequency spectrum. The tentative conclusion is that measurement of ΔZ_{re} is superior to that of ΔZ_{im} for the detection of HSA under these conditions. Since ΔZ_{re} represents the change in resistance of the virus-PEDOT layer, and ΔZ_{im} is the change in the quantity $(\omega C)^{-1}$ where ω is the angular frequency and C is the capacitance, for the resistance of the virus-PEDOT bioaffinity layer, we conclude that the resistance of the virus-PEDOT layer is preferentially perturbed by HSA binding, relative to the capacitance.

The extension of these EIS measurements to a range of HSA concentration from 50 nM to 5 μM (Figure S3) confirms that ΔZ_{re} increases monotonically with HSA concentration from 50 nM to 5 μM. In addition to sensitivity and signal-to-noise, the speed of biosensor response is also critically important. Real time measurements of ΔZ_{re} at f = 340 Hz (Figure 5) show that increasing the HSA concentration in the flow cell causes a prompt increase in ΔZ_{re} on the 5 s time scale followed by a slower increase in ΔZ_{re} over the next 200 s or so. Using the slower of these two time scales, a single measurement comprising exposure to buffer and then to sample can be accomplished in ≈8−10 min.

The sensor-to-sensor reproducibility for HSA detection can be assessed by making repetitive measurements of HSA at a particular concentration using different sensors. The impedance versus frequency data shown in Figure 6a (for ΔZ_{re}) and Figure 6b (for ΔZ_{im}) show error bars representing coefficient-of-variation (COV) for measurements at three different biosensors at each concentration. For ΔZ_{re} in the frequency range from 200 to 500 Hz, no overlap of these error bars occurs between the seven concentration plots, suggesting that the biosensor cleanly resolves these seven concentrations. COV values are minimized for all concentrations in the 200−500 Hz window (Figure 6c) and equal to 2−35% across this frequency range, and for HSA concentrations from 50 nM to 2 μM. For ΔZ_{im} on the other hand, error bars overlap across the frequency spectrum (Figure 6b), and larger COV values apply (Figure 6d) demonstrating again that ΔZ_{im} is a less effective discriminator of HSA than ΔZ_{re}.

While Figure 6a shows that ΔZ_{re} progresses to higher values as the HSA concentration increases, one can ask whether this progression conforms to the Hill equation, which is expected to model the sensor response:[21]

DOI: 10.1021/acs.analchem.6b04840
Anal. Chem. 2017, 89, 1373−1381

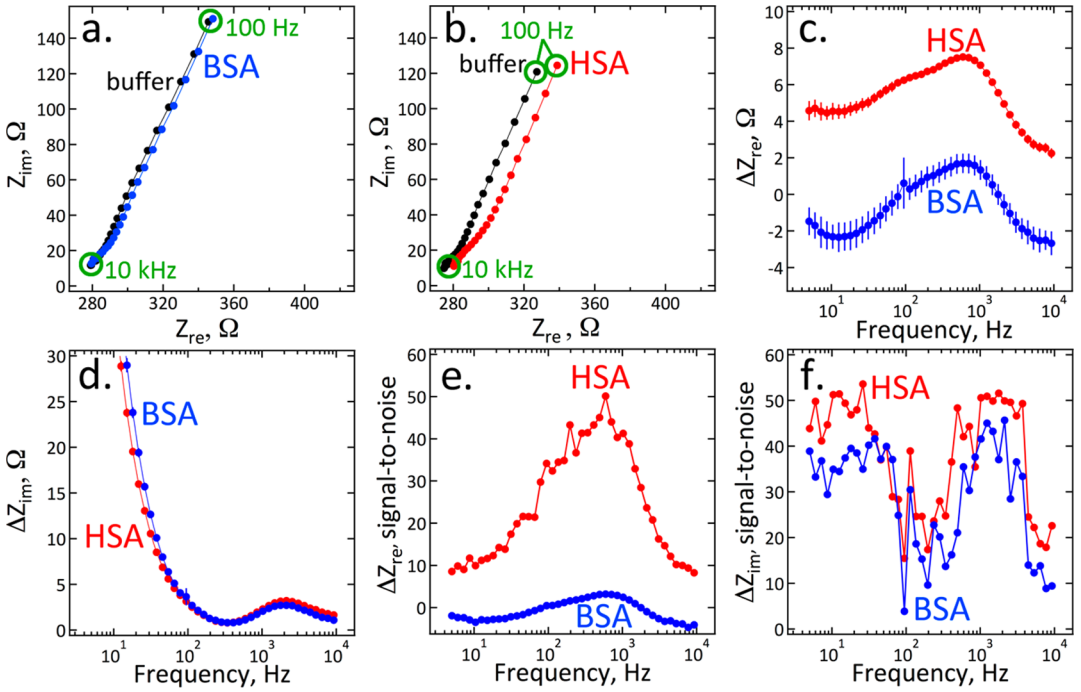

Figure 4. Detection of HSA binding using electrochemical impedance spectroscopy (EIS). The EIS response of virus-PEDOT biosensors upon exposure to 500 nM BSA (blue) and 500 nM HSA (red) is compared. No redox species are added to the solution in these measurements. Error bars represent the standard deviation, $\pm 1\sigma$, of five consecutive EIS measurements on a single electrode. (a, b) Nyquist plots for virus-PEDOT films in solutions of run buffer (black) and 500 nM BSA or HSA. Plots of (c) ΔZ_{re} and (d) ΔZ_{im} versus frequency, where ΔZ is defined as $Z_{analyte} - Z_{buffer}$. Corresponding (e) ΔZ_{re} and (f) ΔZ_{im} signal-to-noise ratio, defined as $\Delta Z/\sigma$, as a function of frequency.

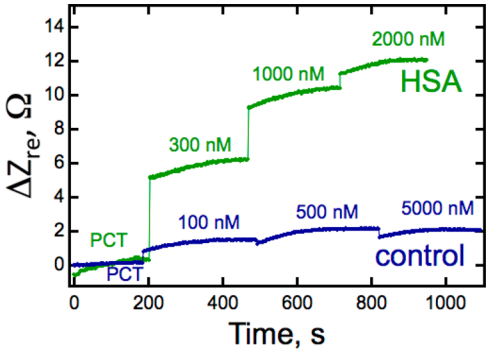

Figure 5. Real time HSA biosensing. Plot of ΔZ_{re} versus time, of a single virus-PEDOT electrode when exposed to three concentrations of HSA, using a control virus that did not bind HSA (blue) and HSA virus (green). A freshly electrodeposited virus-PEDOT film was first immersed in run buffer (PBS-casein-Tween) until an equilibration signal was reached. The time scan was then paused, and five EIS spectra were acquired in rapid succession. Immediately following this, the virus-PEDOT film was exposed to 100 nM HSA in run buffer, and the time scan was restarted within 5 s of exposure. This procedure was repeated for exposures to 500 and 5000 nM HSA.

$$\Delta Z_{re} = \Delta Z_{re,lim} + \frac{\Delta Z_{re,0} - \Delta Z_{re,lim}}{1 + \left(\frac{C_{HSA}}{K_D}\right)^h} \quad (1)$$

Here, the following abbreviations apply: $\Delta Z_{re,lim}$ is the limiting ΔZ_{re} seen at high HSA concentrations, $\Delta Z_{re,0}$ is the minimum value of ΔZ_{re} seen at low C_{HSA}, and K_D is the dissociation constant, which corresponds to the value of C_{HSA} at which $\Delta Z_{re} = (\Delta Z_{re,0} - \Delta Z_{re,lim})/2$. The Hill coefficient, h, equals 1.0 when no cooperativity is present; it has a positive value when positive cooperativity is operating (that is, $K_{D,app}$ increases with HSA loading), and it has a negative value when negative cooperativity is indicated.[21] The R^2 value computed for the best 4-parameter fit of eq 1 to the data of Figure 6a is plotted in Figure 6e. An R^2 value > 0.9 is seen for all frequencies below 800 Hz, and $R^2 > 0.95$ is observed in the frequency range 200–500 Hz (yellow). The calibration of phage-PEDOT biosensors was determined at a single frequency selected to maximize the signal-to-noise ratio, minimize the COV, and provide the highest R^2 value for fits of the Hill equation to our calibration data. On the basis of these three criteria, the frequency selected was 340 Hz. Using f = 340 Hz, for example, the ΔZ_{re} versus C_{HSA} calibration curve shown in Figure 6f is obtained. Hill equation fit parameters for ΔZ_{re} are summarized in Table 2. The Hill coefficient of $h = 1.0 \pm 0.2$ indicates that there is no cooperativity in phage-HSA binding, consistent with previous studies.[11]

Nonspecific adsorption is well-controlled by casein blocking of these virus-PEDOT films. Blue data points in Figure 6f are BSA while green and black data points represent measurements of HSA conducted using a stop 4 virus which has no measurable affinity to HSA (green), and a pure PEDOT film containing no virus (black). Virus-PEDOT films do show slight nonspecific binding to BSA. Therefore, a conservative limit-of-detection for virus-PEDOT films is 100 nM HSA. Corresponding COV values for 100 nM to 5 μM HSA are within 2–8%. Nonspecific binding is attributed to electrostatic interactions between proteins and the positively charged PEDOT backbone. The isoelectric point of HSA and BSA is ~5, rendering the proteins negatively charged in solutions with pH values above 5 such as buffer solutions (pH = 8) used in virus-HSA sensing. Figure S4 demonstrates that lowering the pH of buffer solution suppresses the negative charge on BSA and results in a decrease

DOI: 10.1021/acs.analchem.6b04840
Anal. Chem. 2017, 89, 1373–1381

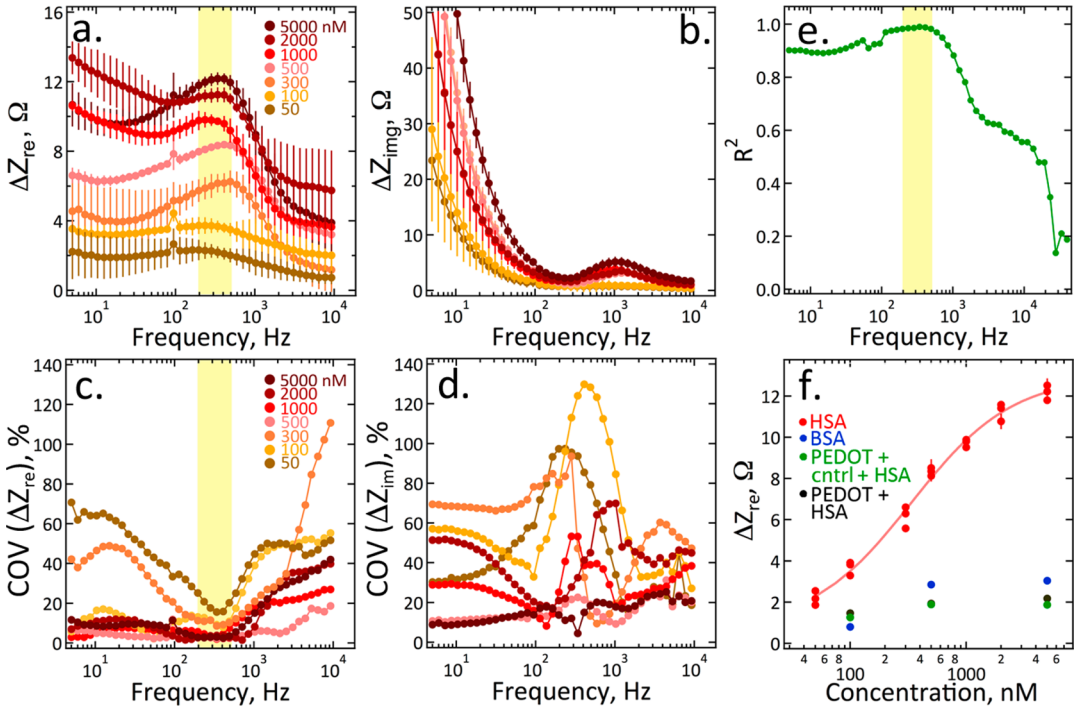

Figure 6. Sensor-to-sensor reproducibility of HSA detection. Calibration plot of (a) ΔZ_{re} and (b) ΔZ_{im} versus frequency for multiple virus-PEDOT films exposed to varying concentrations of HSA. ΔZ values for $n = 3$ independent virus-PEDOT electrodes were averaged to obtain each curve, errors bars indicate $\pm 1\sigma$. Corresponding coefficient of variation, defined as the relative standard deviation for $n = 3$ virus-PEDOT electrodes of (c) ΔZ_{re} and (d) ΔZ_{im} versus frequency plots for each HSA concentration. ΔZ_{re} shows regions of COV values <20% while ΔZ_{im} COV values are too high for reliable measurements. At each frequency, ΔZ_{re} versus [HSA] was fitted to the Hill equation and the square of the regression coefficient, R^2, versus frequency plot (e). $R^2 = 1$ represents the best fit of the Hill equation to the data. The highlighted interval in parts a, c, and e indicates the frequency range where ΔZ_{re} signal is largest, COV is at a minimum, and the peak for goodness of fit occurs, respectively. (f) Calibration plot of ΔZ_{re}, measured at 340 Hz, versus concentration. Each data point represents a different virus-PEDOT electrode with error bars defined as the standard deviation, $\pm 1\sigma$, of five consecutive impedance measurements. Impedance data for HSA exposures to virus-PEDOT films containing HSA (red) phage are fitted to the Hill equation (red line). Three controls to confirm specific binding to HAS are shown: BSA exposure to virus-PEDOT films containing HSA binding phage (blue), HSA exposure to virus-PEDOT films containing a control phage having no affinity for HSA (green), and HSA exposure to pure PEDOT films containing no phage (black).

Table 2. Parameters for the Best Fit of the Hill Equation (Equation 1) to HSA Calibration Curves Acquired in PBS Buffer and Synthetic Urine

	frequency (Hz)	$\Delta Z_{re,0}$ (Ω)	$\Delta Z_{re,lim}$ (Ω)	K_D (nM)	h
PBS	340	0.4 ± 1	12.2 ± 0.5	300 ± 50	1.0 ± 0.2
synthetic urine	136	1×10^{-16} ± 5	15 ± 8	1036 ± 1000	0.5 ± 0.5

of nonspecific binding with the inherently positive PEDOT-only film. The addition of casein blocking solution similarly inhibits nonspecific adsorption compared to sensing in pH 5 buffer. While casein is an effective blocking agent for virus-PEDOT films, it can also block binding sights and suppress sensor response. Such effects are apparent in the observed K_D of virus-PEDOT biosensors, which is slightly higher than K_D = 10−100 nM obtained by ELISA immunosorbent assays.

Detection of HSA in Synthetic Urine. To validate virus-PEDOT sensor capabilities for urine analysis, EIS measurements for HSA detection were repeated in synthetic, buffered urine. Casein blocking was not implemented in synthetic urine sensing experiments. Negative controls in synthetic urine show little nonspecific binding in agreement with previous studies that show synthetic urine improves specificity.[11] Urea disrupts protein interactions and mimics the blocking activity of casein which mitigates the nonspecific binding of HSA and BSA. Virus-PEDOT sensors in synthetic urine demonstrated a concentration dependent response to HSA similar to PBS buffer (Figure 7a). Sensor-to-sensor reproducibility in synthetic urine is maintained at <10% COV centered around 100 Hz (Figure 7b). The optimal frequency point for calibrating virus-PEDOT films in synthetic urine was 136 Hz (Figure 7c) based on the maximum signal-to-noise ratio, minimum COV, and maximum R^2 fits to the Hill equation (Figure S6). Although the impedance responses in synthetic urine and buffer follow a similar trend, assessment of the Hill equation reveals significant differences in the fit parameters (Table 2). In synthetic urine, sensitivity decreases by an order of magnitude, and the Hill coefficient indicates negative cooperativity binding of virus-PEDOT films to HSA. We attribute this to interactions between urea and the PEDOT backbone that induce a reduction-like reaction. Amines participate in a nucleophilic attack on the delocalized positive charge on PEDOT, displacing charge carriers, and decreasing the conductivity of the PEDOT film. The two amine groups on urea enable such interactions with PEDOT to increase the film resistance and ultimately reduce efficiency in impedance sensing toward analytes.[22]

DOI: 10.1021/acs.analchem.6b04840
Anal. Chem. 2017, 89, 1373−1381

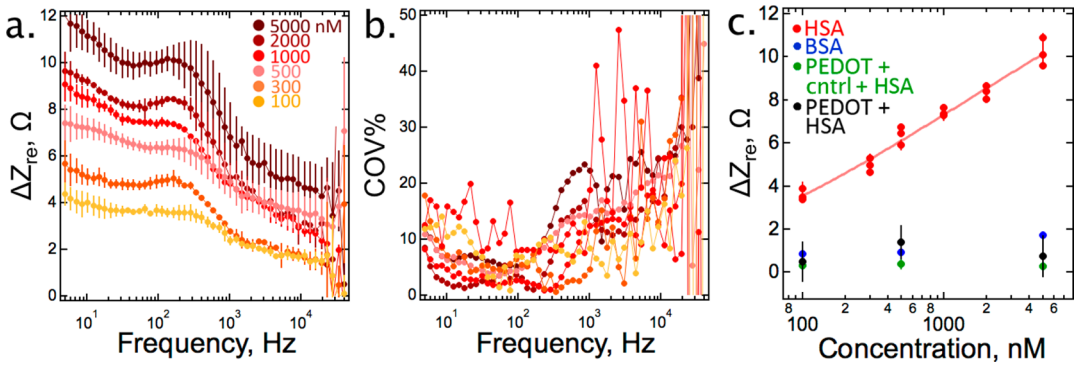

Figure 7. Virus-PEDOT sensors in synthetic urine. Calibration plot of (a) ΔZ_{re} versus frequency for multiple virus-PEDOT films exposed to varying concentrations of HSA. ΔZ values for $n = 3$ independent virus-PEDOT electrodes were averaged to obtain each curve, errors bars indicate $\pm 1\sigma$. (b) Corresponding coefficient of variation (COV), defined as the relative standard deviation for $n = 3$ virus-PEDOT electrodes of ΔZ_{re} versus frequency plots for each HSA concentration. (c) Calibration plot of ΔZ_{re}, measured at 136 Hz, versus concentration. Each data point represents an independent virus-PEDOT electrode with error bars defined as the standard deviation, $\pm 1\sigma$, of five consecutive impedance measurements. Impedance data for HSA exposures to virus-PEDOT films containing HSA (red) phage are fitted to the Hill equation (red line). Three controls to confirm specific binding to HSA are shown: BSA exposure to virus-PEDOT films containing HAS phage (blue), HSA exposure to virus-PEDOT films containing a control phage that did not bind HSA (green), and HSA exposure to pure PEDOT films containing no phage (black).

SUMMARY

We describe a simple, monolithic, two-electrode electrochemical biosensor for the label-free detection of HSA in PBS buffer and synthetic urine. This biosensor relies upon virus-PEDOT bioaffinity layers that are electrodeposited on both electrodes. An EIS measurement of the shift in Z_{re} at an optimum frequency of ≈300 Hz is then used to transduce the binding of HSA. HSA concentrations in a physiologically relevant range of 100 nM to 5 μM were detected using this biosensor. The resulting calibration curves are well-described by the Hill equation for receptor−ligand binding. These single-use biosensors exhibit a sensor-to-sensor reproducibility characterized by a coefficient-of-variation of 2−8% across the entire concentration range. It is also demonstrated that phage-PEDOT biosensors are capable of HSA quantitation in synthetic urine. This simple biosensor architecture is readily manufacturable, is compatible with small sample volumes (≈ 50 μL), and affords rapid analysis times (<15 min). All of these attributes provide motivation for the further development of this and related biosensing technologies.

ASSOCIATED CONTENT

Supporting Information

The Supporting Information is available free of charge on the ACS Publications website at DOI: 10.1021/acs.analchem.6b04840.

Additional materials and methods, photolithography flowchart, phage selections and characterization, equivalent circuit data, and synthetic urine data (PDF)

AUTHOR INFORMATION

Corresponding Authors

*E-mail: gweiss@uci.edu.

*E-mail: rmpenner@uci.edu.

ORCID

Reginald M. Penner: 0000-0003-2831-3028

Notes

The authors declare the following competing financial interest(s): The biosensor described here has been licensed to PhageTech, a company co-founded by Drs. Penner and Weiss. PhageTech is developing products related to the research described here. The terms of this arrangement have been reviewed and approved by the University of California, Irvine in accordance with its conflict of interest policies.

ACKNOWLEDGMENTS

R.M.P gratefully acknowledges the financial support of this work by the National Science Foundation, Chemistry Division through contract CHE-1306928. G.A.W. and R.M.P. acknowledge support from the National Cancer Institute of the NIH (1R33CA206955-01), PhageTech Inc (PHAGE-203015), and Chao Family Comprehensive Cancer Center, UC Irvine. FE-SEM data were acquired using instrumentation of the LEXI facility (http://lexi.eng@uci.edu/) at UCI.

REFERENCES

(1) Beekwilder, J.; Rakonjac, J.; Jongsma, M.; Bosch, D. *Gene* **1999**, *228*, 23−31.
(2) Pacheco, S.; Canton, E.; Zuniga-Navarrete, F.; Pecorari, F.; Bravo, A.; Soberon, M. *AMB Express* **2015**, *5*, 73.
(3) Hayhurst, A.; Georgiou, G. *Curr. Opin. Chem. Biol.* **2001**, *5*, 683−689.
(4) Weiss, G. A.; Penner, R. M. *Anal. Chem.* **2008**, *80*, 3082−3089.
(5) Petrenko, V. A.; Vodyanoy, V. J. *J. Microbiol. Methods* **2003**, *53*, 253−262.
(6) Nanduri, V.; Sorokulova, I. B.; Samoylov, A. M.; Simonian, A. L.; Petrenko, V. A.; Vodyanoy, V. *Biosens. Bioelectron.* **2007**, *22*, 986−992.
(7) Ionescu, R. E.; Cosnier, S.; Herrmann, S.; Marks, R. S. *Anal. Chem.* **2007**, *79*, 8662−8668.
(8) Arter, J. A.; Diaz, J. E.; Donavan, K. C.; Yuan, T.; Penner, R. M.; Weiss, G. A. *Anal. Chem.* **2012**, *84*, 2776−2783.
(9) Arter, J. A.; Taggart, D. K.; McIntire, T. M.; Penner, R. M.; Weiss, G. A. *Nano Lett.* **2010**, *10*, 4858−4862.
(10) Donavan, K. C.; Arter, J. A.; Pilolli, R.; Cioffi, N.; Weiss, G. A.; Penner, R. M. *Anal. Chem.* **2011**, *83*, 2420−2424.
(11) Mohan, K.; Donavan, K. C.; Arter, J. A.; Penner, R. M.; Weiss, G. A. *J. Am. Chem. Soc.* **2013**, *135*, 7761−7767.
(12) Meigs, J. B.; D'Agostino, R. B.; Nathan, D. M.; Rifai, N.; Wilson, P. W. F. *Diabetes Care* **2002**, *25*, 977−983.
(13) Wu, H. Y.; Peng, Y. S.; Chiang, C. K.; Huang, J. W.; Hung, K. Y.; Wu, K. D.; Tu, Y. K.; Chien, K. L. *JAMA. Int. Med.* **2014**, *174*, 1108−1115.
(14) Chavers, B. M.; Mauer, S. M.; Ramsay, R. C.; Steffes, M. W. *Diabetes* **1994**, *43*, 441−446.

DOI: 10.1021/acs.analchem.6b04840
Anal. Chem. 2017, 89, 1373−1381

(15) Gross, J. L.; de Azevedo, M. J.; Silveiro, S. P.; Canani, L. H.; Caramori, M. L.; Zelmanovitz, T. *Diabetes Care* **2005**, *28*, 164−176.
(16) Viberti, G. C.; Hill, R. D.; Jarrett, R. J.; Argyropoulos, A.; Mahmud, U.; Keen, H. *Lancet* **1982**, *319*, 1430−1432.
(17) Watta, G. F.; B, J. E.; R, D. J.; Morris, R. W.; Gatting, W.; Polak, A. *Clin. Chem.* **1986**, *32*, 1544−1548.
(18) Jones, C. A.; Francis, M. E.; Eberhardt, M. S.; Chavers, B.; Coresh, J.; Engelgau, M.; Kusek, J. W.; Byrd-Holt, D.; Narayan, V.; Herman, W. H.; Jones, C. P.; Salive, M.; Agodoa, L. Y. *Am. J. Kidney Dis.* **2002**, *39*, 445−459.
(19) Sidhu, S. S.; Lowman, H. B.; Cunningham, B. C.; Wells, J. A. *Methods Enzymol.* **2000**, *328*, 333−363.
(20) Huang, B. X.; Kim, H. Y.; Dass, C. *J. Am. Soc. Mass Spectrom.* **2004**, *15*, 1237−1247.
(21) Kurganov, B. I.; Lobanov, A. V.; Borisov, I. A.; Reshetilov, A. N. *Anal. Chim. Acta* **2001**, *427*, 11−19.
(22) Hojati-Talemi, P.; Evans, D.; Fabretto, M. *Chem. Mater.* **2013**, *25*, 1837−1841.
(23) Thakkar, H.; Newman, D. J.; Holownia, F.; Davey, C. L.; Wang, C. C.; Lloyd, J. *Clin. Chem.* **1997**, *43*, 1471−1471.
(24) Sakti, S. P.; Hauptmann, P.; Zimmermann, B.; Buhling, F.; Ansorge, S. *Sens. Actuators, B* **2001**, *78*, 257−262.
(25) Caballero, D.; Martinez, E.; Bausells, J.; Errachid, A.; Samitier, J. *Anal. Chim. Acta* **2012**, *720*, 43−48.
(26) Cieplak, M.; Szwabinska, K.; Sosnowska, M.; Chandra, B. K. C.; Borowicz, P.; Noworyta, K.; D'Souza, F.; Kutner, W. *Biosens. Bioelectron.* **2015**, *74*, 960−966.
(27) Omidfar, K.; Dehdast, A.; Zarei, H.; Sourkohi, B. K.; Larijani, B. *Biosens. Bioelectron.* **2011**, *26*, 4177−4183.
(28) Chuang, Y. H.; Chang, Y. T.; Liu, K. L.; Chang, H. Y.; Yew, T. R. *Biosens. Bioelectron.* **2011**, *28*, 368−372.
(29) Han, L.; Liu, P.; Petrenko, V. A.; Liu, A. H. *Sci. Rep.* **2016**, *6*, 22199.
(30) Wu, Z. S.; Li, J. S.; Deng, T.; Luo, M. H.; Shen, G. L.; Yu, R. Q. *Anal. Biochem.* **2005**, *337*, 308−315.

DOI: 10.1021/acs.analchem.6b04840
Anal. Chem. 2017, 89, 1373−1381